Technical Paper

The effects of particle shape on the yielding behaviour of crushable sand

John de Bono [*], Glenn McDowell

University of Nottingham, UK

Abstract

Discrete element method simulations are used to investigate the effects of particle shape on the plastic behaviour of sand. This is achieved by using four different shapes of crushable particles. The behaviours of the different particles when subjected to isotropic compression, triaxial shearing, and a range of stress path tests are compared, revealing the important role of particle shape on key aspects of behaviour. Yield surfaces are established and analysed with respect to different modes of deformation, and are also shown to depend on the particle shape. A simple state boundary surface is then obtained, which is confirmed by a performing an additional stress path test on a sample that had been sheared to a critical state.

© 2020 Production and hosting by Elsevier B.V. on behalf of The Japanese Geotechnical Society. This is an open access article under the CC BY-NC-ND license (http://creativecommons.org/licenses/by-nc-nd/4.0/).

Keywords: Discrete element method; Particle crushing; Particle shape; Yielding; Micro mechanics; Sand

1. Introduction

By utilising a simple crushing model, it has been possible using the discrete element method to reproduce all important aspects of soil behaviour within the critical state soil mechanics framework. For instance, the discrete element method (DEM) has been used to correctly model and investigate normal compression behaviour and evolving particle size distributions, triaxial shearing behaviour and dilatancy, and the general yielding and hardening of granular soils (e.g. de Bono and McDowell, 2018a, 2018b, 2018c). Such work has led to many insights, however, like the majority of research to date using DEM, this previous work used spheres to model soil particles, a convenient and efficient yet unrealistic simplification.

The shape of real sand grains can vary widely, and particle shape is known to have a large influence on most aspects of behaviour, most obviously the packing properties and bulk frictional behaviour (e.g. Cho et al., 2006). In this work, major aspects of the critical state soil mechanics framework will be revisited using DEM, but using a variety of particle shapes, the effects of which will be summarised. The aim is to shed light on how and why particle shape influences the macroscopic behaviour of a granular soil.

The outline of this paper is as follows: firstly a brief background to the DEM model, outlining the key concepts such as particle breakage, a comment on previous work, and a description of the particle shapes investigated here. This is followed by the results section, which is divided into three subsections: normal compression tests, triaxial tests, and stress path tests. The subsection on stress paths is the largest and includes analysis of yield surfaces obtained for each material, which is reconciled with the behaviour observed in the normal compression and triaxial tests. There then follows a brief conclusion.

2. Background to dem model

The work presented here is performed using the commercial DEM software PFC3D (Itasca, 2015). A brief summary of the key modelling parameters and methods is given here, after which the results of simulations investigating the normal compression, shearing, and yield surfaces of four different particles shapes are summarised and discussed.

All simulations reported on use triaxial samples. That is, each sample tested is enclosed by a flexible cylindrical membrane and two rigid platens, capable of applying any specified combination of axial and radial stresses and strains (further details can be found in (de Bono and McDowell, 2018b) and Table 1). All stresses here should be considered effective (no pore pressure is simulated).

2.1. Particle breakage

There are several general methods to model particle breakage using DEM. One such method is to use model soil grains as 'agglomerates' made up of many smaller spheres, which are bonded together (e.g. Harireche and McDowell, 2002). This has the advantage of easily facilitating realistic fragmentation of individual soil particles, however it is unsuitable for modelling breakage in larger samples comprising thousands of particles due to limitations in the number of spheres, and the fact that each particle contains internal voids. A different method is to model soil particles as single entities and simply replace these with multiple smaller particles when judged to have broken. This allows the simulation of much larger samples with many more particles but is unable to perfectly capture the breakage of individual grains. Two alternative approaches are to replace particles with non-overlapping fragments whilst not obeying conserving mass (e.g. Lobo-Guerrero et al., 2006), or to have temporarily-overlapping fragments which obey conservation of mass (e.g. McDowell and de Bono, 2013), which is the method used here.

One of the key aspects of the authors' current and previous work using DEM is the use of a simple particle breakage model. This uses the average octahedral shear stress in a particle:

$$q = \frac{1}{3}\left[(\sigma_1 - \sigma_2)^2 + (\sigma_2 - \sigma_3)^2 + (\sigma_1 - \sigma_3)^2\right]^{1/2} \quad (1)$$

to determine whether or not a particle breaks. This shear stress is calculated from the average principal stresses (σ_1, σ_2, σ_3) within a particle, which are calculated directly from the contact forces acting on the particle (Itasca, 2015). The average principal stresses take into account all particle contacts, but no consideration is given to internal stress distributions. The contact law used in all simulations is Hertz-Mindlin, using the stiffness parameters given in Table 1. The particles are attributed random strengths according to a Weibull distribution, whereby the average strength q_0 for a given size (d) of particle is:

$$q_0 \propto d^{-b} \quad (2)$$

where b can be described as the size-effect on strength. The average strengths, their distribution and the size-effect used here were all obtained from single-particle crushing tests on a silica sand (McDowell, 2002). That is, average strengths (q_0) were measured for a range of different sizes d, for a real silica sand, which enabled the parameter b to be determined. The value b used here is given in Table 1, as well as q_0 for the initial 2 mm particles. This breakage model has been shown to successfully reproduce the correct normal compression lines and fractal distributions for real sands (de Bono and McDowell, 2018a), and has been used throughout previous work (see de Bono and McDowell, 2016; McDowell and de Bono, 2013 for further details and analysis). When breaking, particles are replaced by two smaller fragments of the same shape, obeying conservation of mass (each fragment has half original volume). These are placed partially and temporarily overlapping, within the original particle space, and are assigned a random strength from a distribution where the average is determined by Eq. (2). The strengths used were obtained from a silica sand, and therefore many of the simulations involve very large stresses, the conclusions however are be applicable to any stress level.

2.2. Particle shapes

A total of four different particle shapes including spheres are used in this study. The three non-spherical particle shapes are modelled using 'clumps', which is the software terminology for a rigid particle consisting of overlapping spheres. These particles have uniform density, and the 'sub-spheres' do not interact with one another. The three types of clumps, consisting of 2 or 3 sub-spheres are illustrated in Fig. 1. Clump A consists of two equal-sized spheres, with an overlap equal to their common radius. Clump B consists of a smaller sphere overlapping a larger one, the smaller sphere is centred on the surface of the larger one, and has half the radius. Clump C has two such smaller spheres, located at opposite poles on the larger sphere. These shapes are not assumed to be realistic, but rather they were chosen as a sensible step beyond the use

Table 1
Key numerical model parameters.

| Initial Sample Parameters	
Nominal sample size (*height × diameter*)	30 × 15 mm
Initial number of particle	744
Initial particle size, d_e	2 mm
Initial average particle strength, q_0	37.5 MPa
General Model Properties	
Particle shear modulus, G	28 GPa
Particle Poission's ratio	0.25
Size-effect on particle strength, b ($q_0 \sim d^{-b}$)	≈1
Particle friction coefficient	0.5
Damping coefficient	0.7
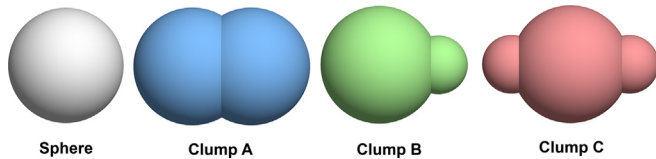
Fig. 1. Different particle shapes used in this study.

of spheres. Even though the particle shapes are still relatively simplified, their increased abilities to interlock and resist rolling are more realistic compared to spheres. Images and shape analyses of real sand grains may be found in Mitchell and Soga (2005) or in the work of Coop et al. (e.g. Altuhafi and Coop, 2011).

The starting point for all work here is a single sample of each different particle shape, i.e. four samples. Each sample had the same number of initial particles (7 4 4). The initial spheres had diameters of $d = 2$ mm; the initial clumps were created with the same volume as these spheres. In other words, the initial clumps had *equivalent spherical diameters* of 2 mm. The equivalent spherical diameter, d_e, of any volume is the diameter of a sphere with the same volume, and will be used throughout this work when referring to the size of the clumps.

When any of the particles was deemed to have broken, it was replaced by two smaller, identically-shaped fragments, obeying conservation of mass. For the clumps, these fragments were placed transversely along the longitudinal axes, to minimise any temporary overlaps with each other and any surrounding particles (the placement of fragments has no observable effects in the simulations (McDowell and de Bono, 2013)). Sphere fragments were placed along the direction of the minor principal stress.

In reality one might expect the clumps to preferentially fracture across one of the 'necks' between spheres, and to produce different shape fragments. However to implement such a procedure in DEM, for multiple generations of fragments is very problematic (as is implementing any form of breakage). The simplified approach here, where breaking particles are replaced by two smaller fragments of the same shape, allows fragments to continue breaking as many times as needed with ease, and also allows us to completely isolate the effects of particle shape before, during and after yielding. This is also consistent with experimental studies which have shown that crushing tends to reduce heterogeneity in shapes (Bowman et al., 2001; Yan and Shi, 2014); as well as observations of fractal distributions produced from crushing, which demonstrate self-similarity across scales. This work should therefore be considered a sensible next step from using just spheres. Previous investigations involving this breakage model also showed that the number of fragments produced following breakage has no effect on the macroscopic behaviour (McDowell and de Bono, 2013).

3. Results

3.1. Normal compression

Isotropic normal compression tests were performed by applying isotropic stress increments via the membrane and platens (whilst allowing particles to break indefinitely). The normal compression results for the four particle shapes are presented in Fig. 2. All materials exhibit the same compressibility, i.e. the same slope. This is due to the materials having the same size-effect on particle strength (the slope of the compression line is a function of the hardening rate (de Bono and McDowell, 2018a)). The four materials all have the same volume of solids, but different initial voids ratios. Upon confinement, the clumps all pack more efficiently than the spheres, with clumps A exhibiting the lowest initial voids ratio. This happens to be consistent with research on packing which has found that prolate ellipsoids with an aspect ratio of ≈ 1.5 are inherently able to form the densest random packing (Donev, 2004).

The different materials appear to have remarkably different apparent yield stresses, despite all having the same particle strengths. The difference in observed yield stresses in these tests is due to crushing beginning at different points during the tests in each material. This can be seen in Fig. 3 (a), which shows the total number of particles in each test against the applied stress. All simulations demonstrate the same rate of increase in particles with increasing stress (the lines are parallel), which is due to the size-effect on particle strength being the same. At any given applied stress the total number of particles is dependent on the particle shape—the separation between the lines is due to an earlier or later onset of crushing. The initial onset of breakage is very brittle due to the initial mono-dispersity, however
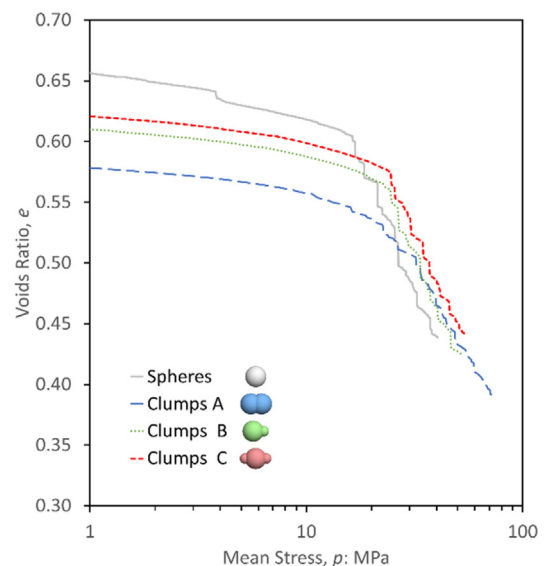

Fig. 2. Normal compression results.

the underlying behaviour is clear: crushing begins earliest in the spheres, and latest in clumps A. At the end of the simulations, all tests contain approximately 30 000 particles, with similar fractal distributions, shown in Fig. 3(b). An image showing the Clump B sample after the test is shown in the inset in Fig. 3(b).

Experimentally, it has been observed that for a given granular material (assuming approximately constant particle shape), looser samples yield at lower stresses than denser samples, and that such samples of different initial densities typically merge to a single compression line following yield (Hagerty et al., 1993; Nakata et al., 2001; Pestana and Whittle, 1995). This earlier yielding of looser samples has often been attributed to lower coordination numbers giving rise to greater induced particle stresses, however, previous analysis using DEM (de Bono and McDowell, 2015) suggested that the apparent earlier yielding in looser samples is mainly due to the larger initial voids, which give a greater potential for voids reduction, with a negligible difference in the quantity or onset of breakage when comparing loose and dense samples of the same material. Furthermore, for real sands there is generally a constant particle shape between different samples, which is clearly not applicable to the simulations.

The macroscopic yield stress observed in normal compression tests on real sands has been linked to the average particle strengths (McDowell, 2002; Nakata et al., 2001). In the simulations, it can be seen that the materials begin to undergo major crushing (i.e. yielding) at different stages despite having the same average particle strengths. The different particle shapes give rise to significantly different contact distributions, which in turn influence the particle stresses. It is known that for yielding and significant volumetric strains to occur, a sufficient number of particles must break. At the start of the simulations, the samples only contain a single size of particle: Fig. 4(a) plots the average shear stress in these initial (and largest) particles ($d_e = 2$ mm), plotted against volumetric strain. The average stresses increase approximately linearly until breakage occurs. The samples all undergo yielding at strains of around $\varepsilon_v = 3$–4%, at which point the rate of increase in average particle stress greatly reduces with the onset of major crushing. What is notable is that the particles display different average stresses during and after yielding. The sphere simulation yields under the lowest average particle shear stress (around 12–13 MPa) while the clump simulations all demonstrate greater values.

The clumps' ability to bear greater average shear stresses compared to the spheres suggests that the clumps provide a more stable, uniform load distribution, and experience less extreme particle stresses. This is reflected in Fig. 4(b), which shows the average coordination numbers (for all particles) from the four simulations: the clumps demonstrate higher average coordination numbers than the spheres throughout the tests. An increased number of average contacts per particle mitigates against extreme particle shear stresses, providing a more homogeneous distribution of forces chains. This enables the aggregate of clumps to sustain a larger macroscopic stress before initiating particle breakage, and therefore 'delays' the onset of breakage— larger applied stresses are needed to initiate fracture and therefore achieve volume reduction, giving a larger macroscopic yield stress.

Figs. 2–4 suggest that for each particle shape, there appears a correlation between average coordination number, the induced particle shear stresses, and the amount of breakage at any given stress. The effect of shape therefore appears to be as equally significant as the particles' crushing strength in governing the compressive behaviour: clumps A have an apparent yield stress approximately
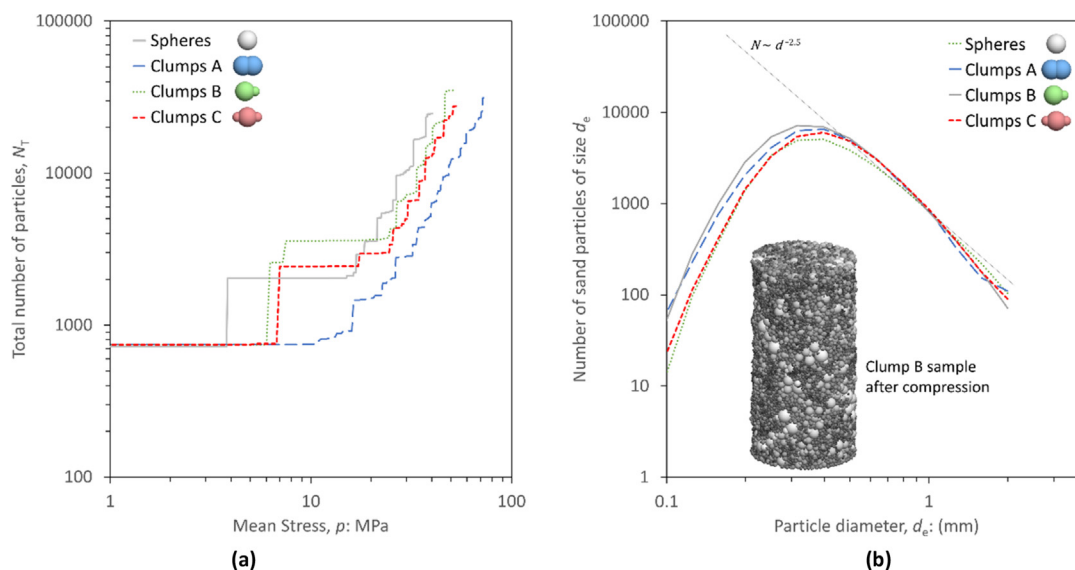

Fig. 3. Total number of particles (a) and final size distributions (b).
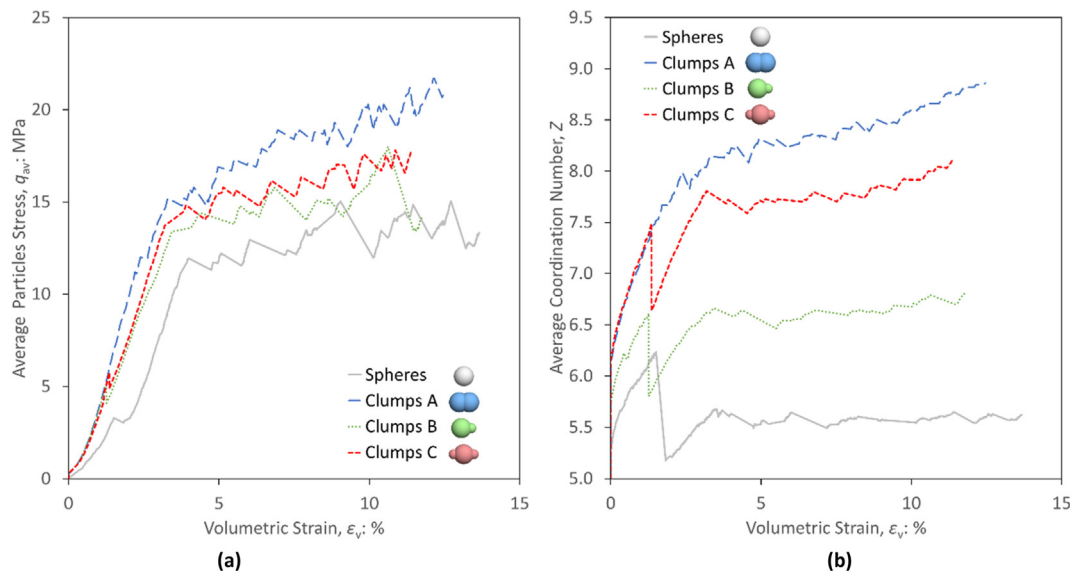
Fig. 4. Average particle stress (a) and average coordination number (b) as functions of volumetric strain.

double that of the spheres, despite having the same strengths, due to their geometry.

3.2. Triaxial shearing

The varying abilities of the four particle shapes to form and maintain contacts will also have an effect on the shear strength, which will be briefly examined in this section using triaxial shear tests. Taking into account the different isotropic yield stresses of the materials, it was chosen to compare triaxial tests performed from normally consolidated states at which the samples have approximately the same number of particles (as opposed to the same stress). The shearing behaviour and critical state line of the spheres has previously been thoroughly examined (de Bono and McDowell, 2018b), by means of 27 triaxial tests on compacted, normally consolidated, and overconsolidated states. This included constant-σ_3, constant-p' and constant-volume tests, and resulted in a well-defined critical state line, which was parallel to the normal compression line. To minimise computational time, only a single representative test was performed here for each clump, which are compared to the equivalent sphere simulation. Constant-volume triaxial simulations were performed on normally consolidated states at which each sample contained approximately 6000 particles. The different compressibility of each particle shape meant that different stresses were needed to achieve samples with approximately this same number of particles (mean stresses of between 24 MPa and 40 MPa). The triaxial tests were performed by applying axial strain increments whilst adjusting the confining pressure so as to achieve a constant volume.

Fig. 5(a) and (b) show the stress–strain results from the constant-volume tests for each material, and Fig. 5(c) shows the stress paths in *q-p*' space (in this plot, the data has been 'smoothed' for clarity using a moving average

technique (de Bono and McDowell, 2018b)). All simulations demonstrate contractile behaviour, which in these tests manifests itself as a decrease in the mean stress *p*, followed by a slight dilative tendency at large strains, typical for such 'undrained' tests on sands (Been and Jefferies, 1985). As elaborated in earlier work (de Bono and McDowell, 2018b), the spheres reached critical states (continuous shearing with no further change in stresses or volume), and demonstrate a critical state constant *M* of around 0.7. It is immediately clear that the clumps have a greater frictional shear resistance, with the clumps A and C both displaying the highest value of *M*≈1 at the end of the tests as they approach critical states (in the figure, the ultimate states have been assumed critical). The difference in shear strengths correlate with the capacity of each particle shape to form contacts: clumps A demonstrate the highest average coordination number, whilst the spheres the lowest. The average coordination numbers measured during the triaxial tests are shown in Fig. 6, showing how the coordination number decreases to a stable value towards the critical state in all tests, and with the same overall observation as Fig. 4(b) whereby the spheres have the fewest contacts and clumps A have the most, followed by clumps C. The difference in coordination numbers between clumps A and C, which both have the same shear strength (*M*≈1), shows that while the capacity to form contacts provides a good indication of shear the strength, the resistance to shear must also be influenced by other geometrical properties. Clumps C are slightly more angular, and possess different rotational inertias, which are likely to play a role.
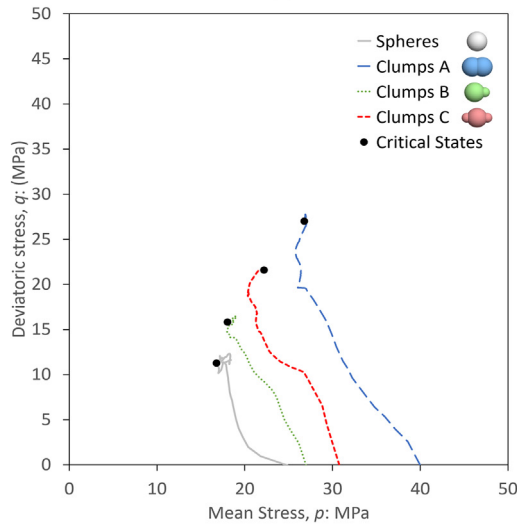
The decrease in average coordination number observed in all constant-volume tests is consistent with previous observations (de Bono and McDowell, 2018b), and suggests that the samples are packed less efficiently, despite the contractile behaviour. This is caused by crushing, without
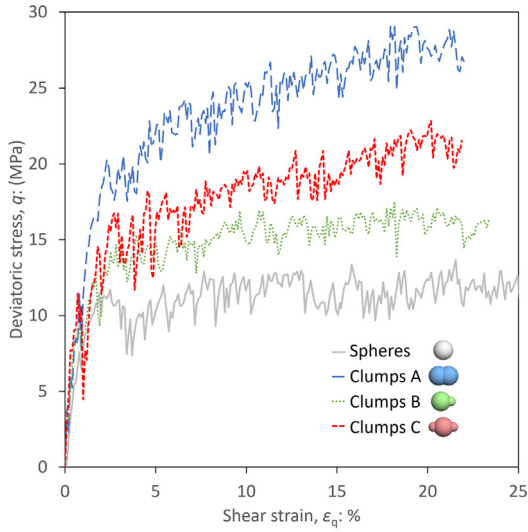
(a)
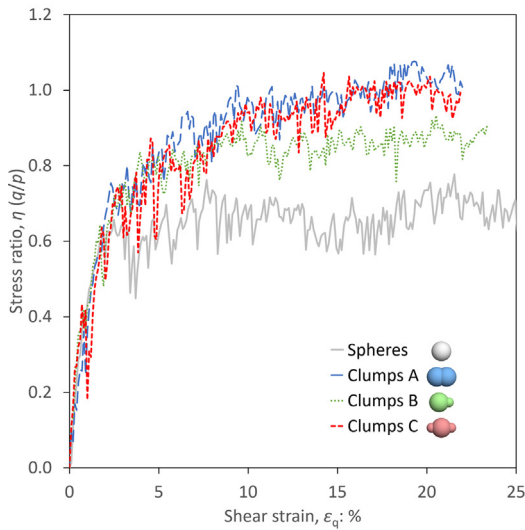
(b)

(c)

Fig. 5. Constant-volume triaxial results: deviatoric stress versus shear strain (a), stress ratio (b) and stress-paths (c).
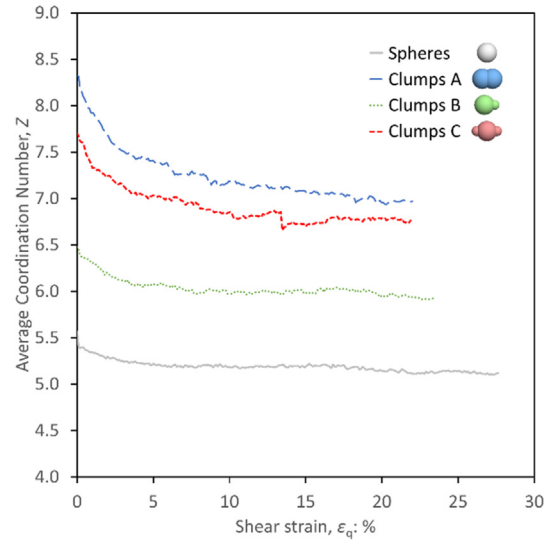

Fig. 6. Coordination number during triaxial shearing.

which it is not possible to achieve contractile behaviour in DEM. To show the crushing that occurs, the total number of particles in each test is plotted against shear strain in Fig. 7(a). All simulations show a rapid initial increase up to $\varepsilon_q \approx 2\%$, after which the quantity of particles increases at an approximately steady rate. Thus the number of particles increases continually with shear strain, despite the samples reaching steady stress states. However, the residual rate of increase is the relatively small particles crushing and continuing to crush, which is evident in Fig. 7(b). This shows the total particle surface area in terms of percentage against shear strain. The rate of increase in particle surface area can be seen to reduce, showing that the particles continuing to break must be getting smaller. In other words, crushing occurs towards the fine end of the particle size distribution. The reason that this continuing breakage has no apparent effect on the volumetric behaviour (or in these 'undrained' simulations, the mean stress) is due to the fact that for volume change to occur, particles of all sizes must break, rather than only the smallest (which will be demonstrated more clearly in the following sections). Another observation is that the rate of breakage during shearing appears to correlate with the stress level—clumps A, sheared under the greatest stress, exhibit the most rapid increase in the number of particles; whilst the spheres, sheared under the lowest stress, exhibit the least rapid increase with shear strain. This is despite the varying stress levels resulting in approximately identical levels of crushing (i.e. ≈ 6000 particles) during normal compression.

3.3. Stress path tests

3.3.1. Background

To investigate yielding and establish and compare the yield surfaces of the materials, series of stress path tests
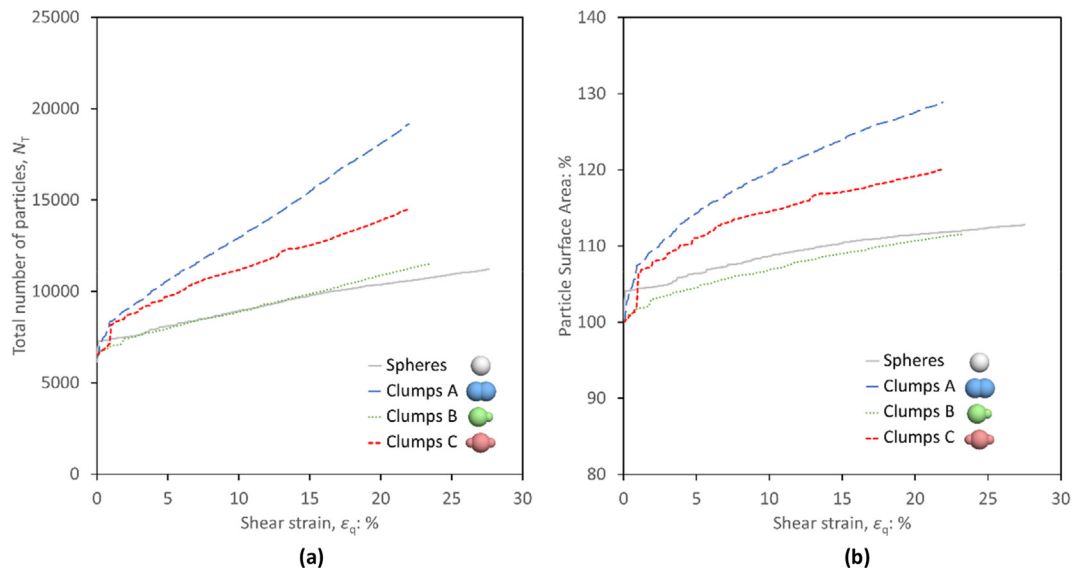
Fig. 7. Total number of particles (a) and total particle surface area (b).

were performed. A previous state-boundary surface obtained from triaxial tests on spheres using DEM gave a clear indication of two separate yield surfaces, consistent with what has been observed for sands (e.g. Chandler, 1985; Vermeer, 1978; Wood, 1990). This prompted further examination of the yield surface, whereby stress path tests (probes) were performed on samples with different stress histories.

Two distinct basic modes of deformation and yielding were characterised and then investigated (de Bono and McDowell, 2018c). Each mode of yielding was associated with a distinct yield surface, which is idealised here in Fig. 8(a). The first type of yielding, which could be considered as frictional yielding, occurred under increasing magnitude of stress ratio $|\eta|$, at relatively low mean stress levels, and was characterised by a gradual change in the macroscopic deviatoric response from stiff to less stiff behaviour. The deviatoric responses from stress probes at relatively low mean stress levels appeared to be a unique function of stress ratio η, i.e. all responses merged into a single η-ε_q curve (for example paths 1 and 2 in Fig. 8). Thus, any interpretation of yielding from this unique response led to a linear yield surface in q-p' space. At significantly greater mean stresses, this 'intrinsic' frictional behaviour was superseded by 'compressive yielding', caused by substantial particle crushing and occurring at lower stress ratios (e.g. paths 3 and 4 in Fig. 8). This type of yielding was characterised by a rapid volumetric contraction, easily identifiable on p-ε_v or e-p plots (Fig. 8(c)). The decrease in volume was caused by major particle crushing, and a subsequent reduction or filling of void space by smaller particles.

The above findings were compared extensively with experimental data for sands (de Bono and McDowell, 2018c), which agreed well, and also revealed insights to anisotropy and kinematic and rotational hardening observed

for real sands. Key results from that work will here be compared to data obtained from similar simulations using the clumps. Specifically, yield surfaces for overconsolidated samples of clumps will be compared to a yield surface for an overconsolidated sample of spheres, all with the same overconsolidation ratio and approximately the same number of particles, and any differences relating to particle shape will be revealed. Each sample was first isotropically compressed until containing approximately 6000 particles, and then (isotropically) unloaded to an overconsolidation ratio of 2.4. From these overconsolidated states, eight stress-controlled stress path tests were performed on each material (e.g. Fig. 9). All stress path tests were stress-controlled, with stress increments of 25 kPa ($= \sqrt{[\delta q^2 + \delta q^2]}$), and were terminated once yielding was deemed to have occurred.

3.3.2. Stress strain results

To illustrate the behaviour, the stress probes on clumps C are shown in Fig. 9(a). Although not shown, crushing occurs in nearly all stress probes, with by far the greatest occurring under large mean stresses. It is worth noting that increasing the deviatoric stress, even when the mean stress decreases (e.g. probe 2), also produces breakage—however this is exclusively fine particles breaking. For analysis of such breakage, including contours of increasing surface area, please refer to previous work using spheres (de Bono and McDowell, 2018c).

The volumetric mean stress responses for clumps C (as an illustrative example) are given in Fig. 9(b) in terms of voids ratio against mean stress p. An abrupt change in the response and decrease in volume ('compressive yielding') is clearly visible for tests 5–8. Defining compressive yielding from these volumetric responses as the onset of permanent volume reduction, indicated by the crosses in the figure, shows that yielding for tests 5–8 occurs across
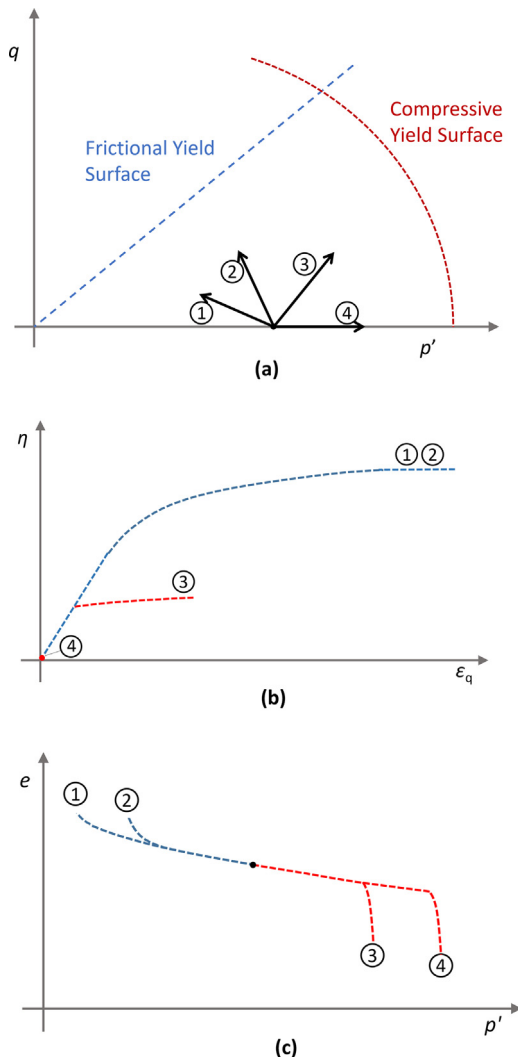
Fig. 8. Diagram showing idealised two modes of yielding: stress paths (a), deviatoric responses (b) and volumetric responses (c).

a range of p values. These yield points lead to a curved compressive yield surface in q-p space (as in Fig. 8), a well-known observation for sand (e.g. Yasufuku et al., 1991).

Fig. 9(c) contains the deviatoric responses, which shows that tests 1–4 merge into a single unique η-ε_q response; demonstrating the 'intrinsic' frictional behaviour of this sample of clumps. This common η-ε_q response for tests 1–4 suggests a linear yield surface, which is consistent with experimental data for sands (Ishihara et al., 1975; Vermeer, 1978). This common η-ε_q response for tests 1–4 means any definition of yielding—for example: the point of maximum curvature, or the end of linearity—will occur at identical values of η. The term 'frictional yielding' is used to refer to any such yielding based on this single intrinsic deviatoric response, for which the behaviour is *not affected by crushing*. Meanwhile, the term 'deviatoric yielding' refers to all observations of yield in the deviatoric response, regardless of whether it is intrinsic behaviour or not (i.e. all tests in Fig. 9(c)).

This unique behaviour and frictional yielding only applies at relatively low mean stresses—once substantial crushing occurs at higher stresses the deviatoric responses deviate from the intrinsic behaviour and demonstrate earlier yielding. This is the case for tests 5–8, which all clearly demonstrate yielding caused by crushing at lower values of η and ε_q. It is important to note however that the compressive yielding observed in Fig. 9(b) does not coincide with the obvious yielding observed in Fig. 9(c). To illustrate this, the crosses in 9(b) have been superimposed in Fig. 9(c). Tests 5–7 demonstrate plastic behaviour in the deviatoric response and deviate from tests 1–4 *before* yielding is observed in the volumetric response. This is caused by substantial crushing of relatively smaller particles, and occurs before the samples demonstrate compressive yielding in Fig. 9(c).

Previous DEM analysis on the mechanisms behind yielding (de Bono and McDowell, 2018c) established that what was unique to compressive yielding is that crushing occurs simultaneously across *all particle sizes*. Specifically, this included the largest particles. In the absence of, or prior to compressive yielding, any crushing that occurs is limited to only the relatively finer particles. That is, a permanent decrease in volume only occurs when particles of all sizes crush. There must be a proportional breakage of all sizes of particles in order to create smaller fragments and enable a denser geometrical packing whilst maintaining an efficient fractal particle size distribution. Thus, compressive yielding, observed from the volumetric response, e.g. the crosses in Fig. 9(b), can be conceptualised as representing the point(s) at which the largest particles begin to break (alongside breakage across all other particle sizes).

For tests 5–7, this means that *i*) any yield surface obtained from the deviatoric responses is no longer linear; and *ii*) the yielding observed in the deviatoric response is distinct from, and not coincident with the compressive yielding observed in the volumetric response. This latter point means that any potential yield point depends on the macroscopic variables used to identify it. This is a known issue for sands, and engineers have often used average or multiple yield points obtained from various stress strain plots to construct a yield surface (Wood, 1990; Yasufuku et al., 1991).

This transitional behaviour has the effect of 'rounding off' the apex or cusp between the two idealised yield surfaces shown in Fig. 8(a), and can be considered as intermediate behaviour, between purely frictional yielding—in which negligible crushing occurs—and purely compressive yielding—in which major crushing of all sizes occurs, facilitating a reduction in volume.

3.3.3. Compressive yield surface

Compressive yielding is associated with breakage of particles of all sizes. The fact that this is preceded by crushing of the relatively finer particles—and that this minor crushing also occurs in the absence of compressive yielding (at low stress)—implies that the largest particles are the most
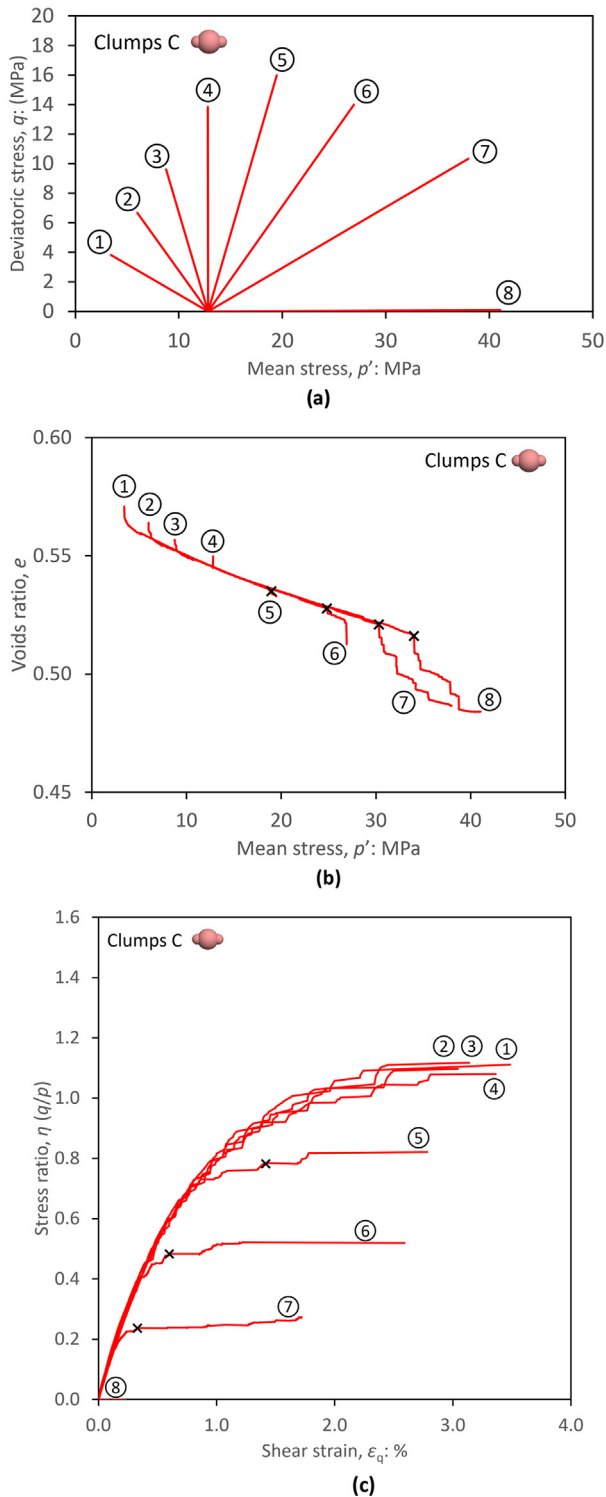
Fig. 9. Stress probes (a), volumetric responses (b) and deviatoric responses (c) for clumps C.

difficult in which to initiate any breakage. It was found previously (de Bono and McDowell, 2018c) that for any given sample, the average stress in the largest particles was approximately constant at compressive yield, irrespective of the stress path. This meant that the shape of the com-

pressive yield surface could be well represented in q-p' space by contours of average particle stress. This is demonstrated in Fig. 10(a) which shows contours of average stress in the largest particles for clumps C (the same observation applies to all materials). The compressive yield points, defined previously in Fig. 9(b), are superimposed again and coincide well with the outermost contour (an average particle shear stress of 16 MPa).

The data for each contour can be normalised by the value of p at which the contour crosses the p-axis, to produce Fig. 10(b). By scaling the contours in this way, any uniqueness of shape can be established. The contours corresponding to larger particle stresses (as the sample approaches yielding) appear coincident in Fig. 10(b) and independent of stress level. To state more clearly, there appears negligible difference between the contours corresponding to average particle stresses of 12–16 MPa. This suggests that the compressive yield surface of a given material has a constant shape, independent of stress level (unlike any shear yield surface). Similar average stress contours for the largest particles are shown for all materials together in Fig. 10(c) in normalised stress space. The values of average shear stress associated with each contour are chosen such that each group of contours share a common point on the p-axis. The purpose of this is to compare the shape of the contours between materials. The contours are largely similar but a consistent trend is visible: the contours for the spheres are the highest (and less curved), whilst those for clumps A and B are consistently lower (more curved). This shows that for a given increase in deviatoric stress (e.g. at a constant p), the average shear stress in the largest particles increases more rapidly in clumps A and B, and less rapidly in clumps C and the spheres. This observation appears to be uniquely determined by the particle shape. There are no obvious correlations with the stress level, average coordination number, voids ratio or frictional strength for each material.

3.3.4. General yield surfaces

For the purpose of comparing, at least qualitatively, the overall yield surfaces for the simulated materials here, a robust definition of yielding is needed which can be applied to all stress probes and therefore not dependent on a single variable. From analysis of plastic strains (not shown) it was deemed that a suitable definition of yield might be the point at which either the deviatoric or volumetric plastic strain exceeds 0.5% ($\max\{\varepsilon_q^p, \varepsilon_v^p\} \geq 0.5\%$) (any threshold value may be used). This arbitrary definition provides a simple and universal method of comparing general yield surfaces, and takes into account yielding observed from any combination of stress and strain variables. The resulting yield surfaces are shown in Fig. 11(a). The section of any yield surface corresponding to shear yielding (i.e. low mean stresses, high stress ratio) appears governed by the frictional strength of the material (M): frictionally-stronger materials display steeper/larger elastic zones. Yielding under isotropic compression, i.e. along the p-axis, is purely
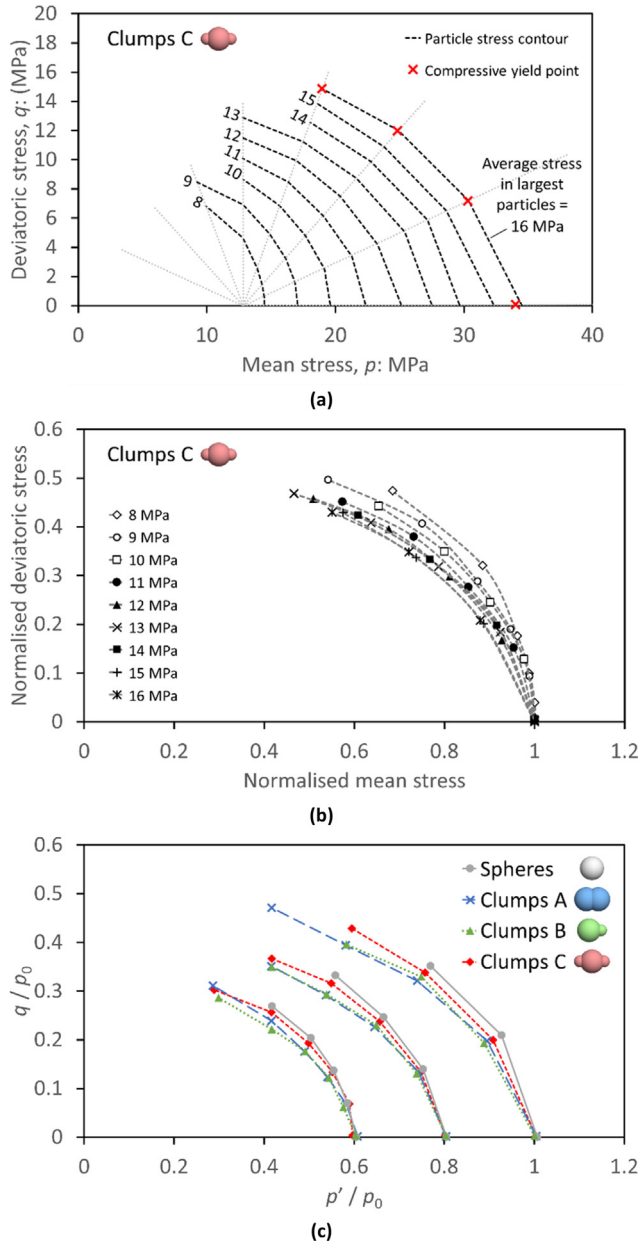
(a)

(b)

(c)

Fig. 10. Contours of average particle stress (a), and the same contours scaled and superimposed (b). Normalised contours for all materials (c).

(a)

(b)

Fig. 11. Yield surfaces according to deviatoric and volumetric plastic strains.

compressive yielding and is determined by the material's stress-history. At intermediate stresses ($0.5 < p/p_0 < 1$) the materials exhibit increasing shear strains, which may or may not be followed by volumetric strains and compressive yielding—see Fig. 9(c).

Fig. 11(b) shows the same yield surfaces normalised by the isotropic yield stress, and reveals clear differences in yield surface shape in the intermediate region ($0.5 < p/p_0 < 1$). This difference in shape is caused by crushing of the relatively finer particles, which is dependent on the magnitude of the applied stresses. To summarise, from analysis of particle breakage and plastic strains, it appears that the yield surface (using the current definition) becomes more rounded with increasing preconsolidation pressure.
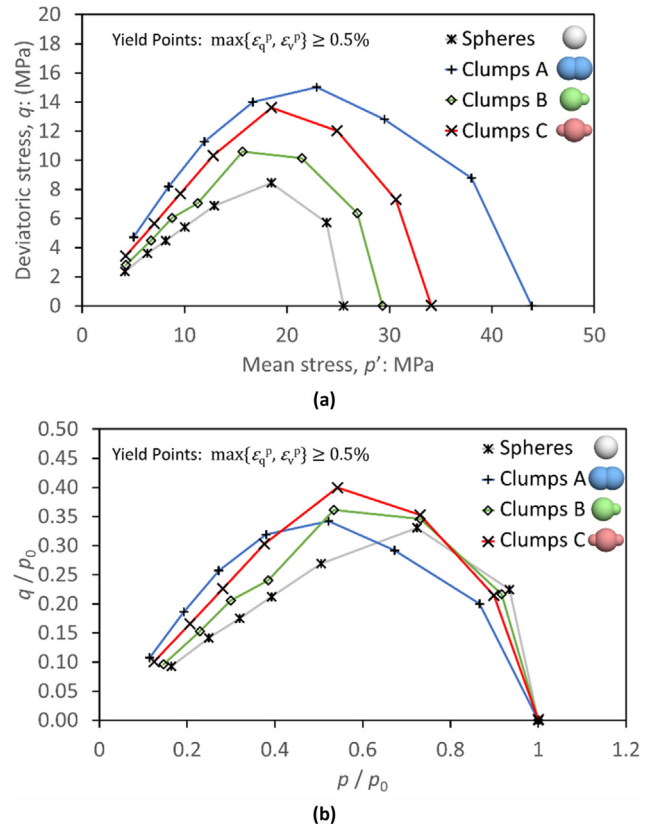
For example, Clumps A have the largest M, but due to the higher stress level for the stress path tests, Clumps A have the most rounded or 'flattened' yield surface. In other words, increasing p_0 causes the normalised yield surface to display greater curvature between the linear frictional section at low stress and isotropic yielding at $p/p_0 \approx 1$.

A general scheme for yielding can be conceptualised as that illustrated in Fig. 12(a). The general deviatoric yield surface(s) depicted in this figure can be based on any arbitrary definition of yield observed from the deviatoric response. Any such deviatoric yield surface is linear at low stresses (corresponding to purely frictional yielding), before becoming curved and tending towards the compressive yield surface at $p \approx p_0$. Each deviatoric yield surface depicted corresponds to a single definition of yielding, such as degradation of shear stiffness or the accumulation of plastic shear strains. On the other hand, the single compressive yield surface depicted in Fig. 12(a) corresponds to the unambiguous yielding observed in the volumetric response for a material.

Fig. 12(b) shows the effects of material and sample properties on the deviatoric and compressive yield surfaces. These double yield surfaces resemble those suggested by Vermeer (1978) and Wood (1990). For any definition of deviatoric yielding, the deviatoric yield surface is directed through the origin, is initially linear, and the incline is lar-
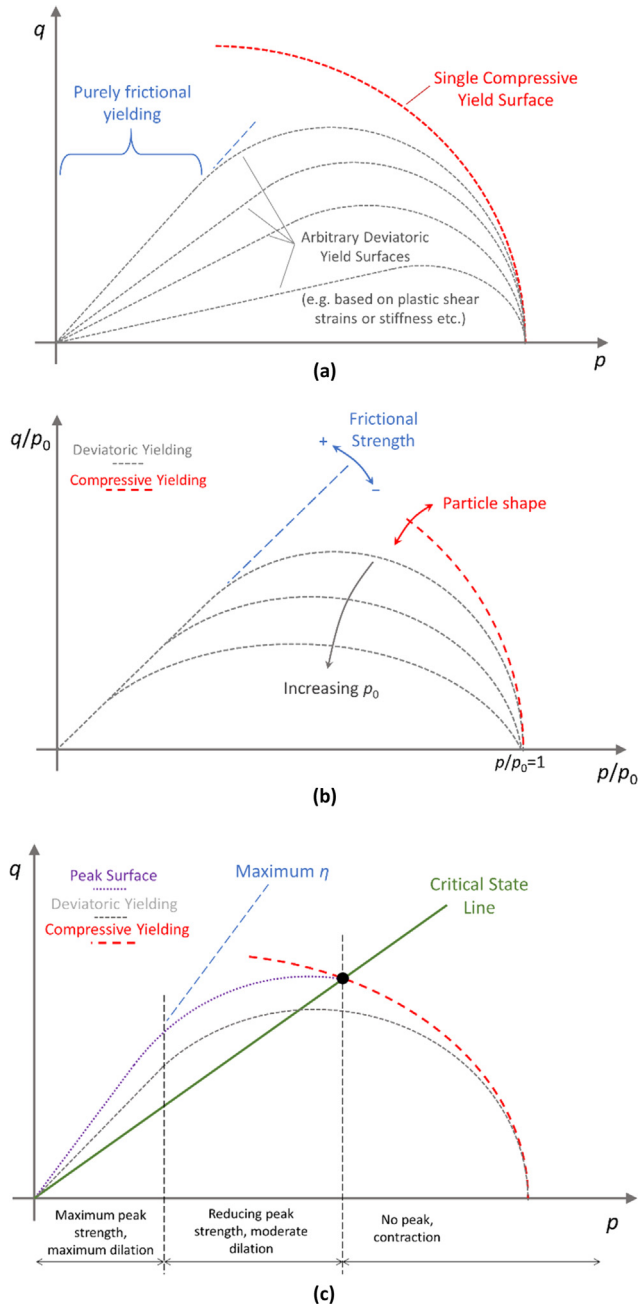
Fig. 12. Generalised yield surfaces: schematic showing frictional yielding, and general deviatoric and compressive yield surfaces (a); schematic showing effects of key parameters on yield surface shape (b); and general yield surfaces shown with respect to triaxial behaviour (c).

gely governed by the frictional strength (M) of the material (as well as the stress history (de Bono and McDowell, 2018c)). The curved section of the shear yield surface depends on both the applied stresses and the location of the compressive yield surface, and is characterised by moderate crushing of relatively fine particles. Therefore the shape of the combined yield surface as a whole is stress-dependent and not constant. The location of the compressive yield surface is defined by the preconsolidation pressure only, and the shape appears a material constant

(e.g. depending on the particle shape). The particle shape clearly influences both the compressive and deviatoric yield surfaces; with further work (with a much wider range of particle shapes) it should be possible to relate these yield surfaces more quantitatively to particle shape parameters (such as sphericity, angularity, etc.).

This general scheme is replotted with reference to triaxial behaviour in Fig. 12(c). Samples of a given material sheared at relatively low pressures will demonstrate a maximum peak stress, the peak envelope being linear in q-p space (at low stresses). As mean stress increases, any arbitrary deviatoric yield surface curves down, and this reflects the reduction in peak strength that is observed under increasing pressures. As can be seen, all samples subjected to shearing (all stress paths except isotropic compression) will demonstrate plastic shear strains and a form of deviatoric yielding before reaching the critical state line. This includes both dilative samples sheared at low pressures, and contractile samples sheared at high pressures, which subsequently undergo compressive yielding and major volumetric contraction. (Only those stress paths which reach the compressive yield surface before the critical state line demonstrate volumetric contraction.) This generalised behaviour was matched exactly by the 27 triaxial results previously performed (de Bono and McDowell, 2018b) using crushable spheres.

3.3.5. State boundary surface

It is clear that any deviatoric yielding is not only highly sensitive to the choice of yield criterion, but also dependent on the stress levels and any changes in direction of the stress path (de Bono and McDowell, 2018c). The compressive yield surface in contrast appears to possess a constant shape which is unique to the material. The fact that the compressive yield surface has a constant shape (a material property) is why the critical state line and normal compression line are parallel in e–$\log \sigma$ space. It is therefore possible to map out a state boundary surface, and/or predict the location of the compressive yield surface from any single known point on the compressive yield surface. An inference from Fig. 12(c) is that any state on the (high-stress) critical state line must also lie on the compressive yield surface. That is, any contractile sample (e.g. normally consolidated) sheared to a critical state must have undergone compressive yielding, and be on the compressive yield surface.

To illustrate this, a compressive 'state boundary' along with the critical state line is shown in Fig. 13(a) for Clumps A. This compressive state boundary is obtained from average particle stress contours, using a similar method to that shown in Fig. 10(b): several particle stress contours obtained from the stress probes are shown together, revealing the unique shape of the compressive yield surface. The critical state line is drawn using $M = 1$, obtained from the triaxial test shown earlier. From this diagram, the normalised mean stress at the critical state is $p_c/p_0 = 0.46$. The mean stress p at the critical state for triaxial test on this material (Fig. 5) is 26.8 MPa, implying that the new
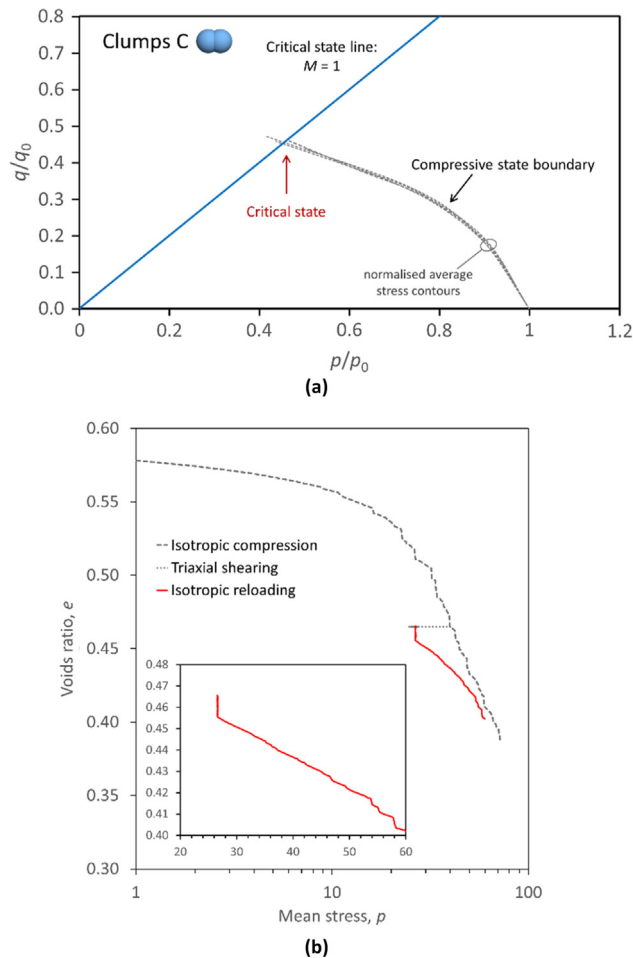
Fig. 13. Normalised compressive yield surface and critical state line for 11 clumps (a), and results for isotropically reloading sample after triaxial shearing (b).

during shearing, and is related to the difference in coordination numbers.

4. Conclusions

This work has compared the general stress–strain behaviour of a set of crushable sands with different particle shapes. When subjected to isotropic normal compression, despite all four particle shapes having the same crushing strengths and properties, the samples demonstrated markedly different yield stresses. Clumps A demonstrated the greatest apparent yield stress, primarily due to a later onset of crushing, in turn primarily due to the particles' ability to form contacts, meaning a more uniform distribution of contact forces and thus were able to bear greater macroscopic stresses.

Triaxial shearing simulations on equivalent samples, with approximately the same number of particles revealed that the clumps exhibited greater shear strengths. During shearing, all samples demonstrated significant breakage, which was most influenced by the applied stress level (p). Thus, the clumps, which required much higher stresses during normal compression to achieve a given level of crushing, then subsequently demonstrated higher rates of crushing during shearing when compared to the spheres, which were sheared under lower mean stresses.

Plastic behaviour and yielding was analysed from both the deviatoric and volumetric responses. The deviatoric responses, no matter what definition of yielding was used, revealed a linear yield surface at low stresses which curved down towards the p-axis at higher stresses as particle crushing became more prominent. Purely 'frictional' yielding at low stresses was characterised by increasing plastic shear strains with negligible crushing. The inclination of this linear region of the deviatoric yield surface was primarily governed by the frictional strength (M) of the material. At higher stresses, deviatoric yielding was characterised by accelerated shear strains caused by particle crushing, which typically preceded more substantial crushing and volumetric contraction. This yielding (and thus the general yield surface for a material) appeared to be dependent on the stress level.

Yielding observed at high stresses from the volumetric responses, i.e. compressive yielding, was associated with major crushing and permanent volumetric strains. The location of the compressive yield surface was defined by the preconsolidation pressure, and the shape depended on the particle shape. The results indicated that the compressive yield surface for each material was a unique shape and independent of stress, meaning it was possible to estimate a compressive state boundary. From the assumption that any (high stress) critical state point must lie on both the critical state line and the compressive yield surface in q-p space, it was possible to estimate the compressive yield surface from a single critical state point. This was confirmed by a simple stress path simulation on the most extensively crushed sample of clumps.

preconsolidation pressure, i.e. the isotropic yield stress is 26.6 / 0.46 ≈ 58 MPa.

After the shearing to a critical state, the Clump A triaxial sample was unloaded to $q = 0$ MPa at a constant mean stress, and then reloaded isotropically. The results for this stress path are given in Fig. 13(b), and clearly show that the sample yields at almost exactly 58 MPa, confirming the shape of the compressive yield surface. This simple method is more useful for predicting the yield stress in isotropic compression than graphically. For example, if the normal compression line is known, one may project a reloading line from any point in e-σ space to estimate the isotropic yield point, however this assumes purely elastic reloading. Following shearing, this is not the case, where plastic strains typically occur (e.g. McDowell et al., 2002): note the volumetric contraction that occurs during unloading of the deviatoric stress in Fig. 13(b). This volume reduction is not due to any significant further breakage, but rather can be considered as a form of kinematic yielding due to changing the stress path direction (de Bono and McDowell, 2018c). Although it is outside the scope of this work, this results from the major crushing that occurred

Acknowledgements

References

Altuhafi, F.N., Coop, M.R., 2011. Changes to particle characteristics associated with the compression of sands. Géotechnique 61, 459–471. https://doi.org/10.1680/geot.9.P.114.

Been, K., Jefferies, M.G., 1985. A state parameter for sands. Géotechnique 35, 99–112. https://doi.org/10.1680/geot.1985.35.2.99.

Bowman, E.T., Soga, K., Drummond, W., 2001. Particle shape characterisation using Fourier descriptor analysis. Géotechnique 51, 545–554. https://doi.org/10.1680/geot.2001.51.6.545.

Chandler, H.W., 1985. A plasticity theory without drucker's postulate, suitable for granular materials. J. Mech. Phys. Solids 33, 215–226. https://doi.org/10.1016/0022-5096(85)90012-2.

Cho, G.-C., Dodds, J., Santamarina, J.C., 2006. Particle shape effects on packing density, stiffness, and strength: natural and crushed sands. J. Geotech. Geoenvironmental Eng. 132, 591–602. https://doi.org/10.1061/(ASCE)1090-0241(2006)132:5(591).

de Bono, J.P., McDowell, G.R., 2018a. Validation of the log e– log σ normal compression law using particle strength data. Géotechnique 68, 451–456. https://doi.org/10.1680/jgeot.17.T.007.

de Bono, J.P., McDowell, G.R., 2018b. Micro mechanics of drained and undrained shearing of compacted and overconsolidated crushable sand. Géotechnique 68, 575–589. https://doi.org/10.1680/jgeot.16.P.318.

de Bono, J.P., McDowell, G.R., 2018c. On the micro mechanics of yielding and hardening of crushable granular soils. Comput. Geotech. 97, 167–188. https://doi.org/10.1016/j.compgeo.2018.01.010.

de Bono, J.P., McDowell, G.R., 2016. Particle breakage criteria in discrete-element modelling. Géotechnique 66, 1014–1027. https://doi.org/10.1680/jgeot.15.P.280.

de Bono, J.P., McDowell, G.R., 2015. An insight into the yielding and normal compression of sand with irregularly-shaped particles using DEM. Powder Technol. 271, 270–277. https://doi.org/10.1016/j.powtec.2014.11.013.

Donev, A., 2004. Improving the density of jammed disordered packings using ellipsoids. Science 303 (80), 990–993. https://doi.org/10.1126/science.1093010.

Hagerty, M.M., Hite, D.R., Ullrich, C.R., Hagerty, D.J., 1993. One-dimensional high-pressure compression of granular media. J. Geotech. Eng. 119, 1–18. https://doi.org/10.1061/(ASCE)0733-9410(1993)119:1(1).

Harireche, O., McDowell, G.R., 2002. Discrete element modelling of yielding and normal compression of sand. Géotechnique 52, 299–304. https://doi.org/10.1680/geot.2002.52.4.299.

Ishihara, K., Tatsuoka, F., Yasuda, S., 1975. Undrained deformation and liquefaction of sand under cyclic stresses. Soils Found. 15, 29–44. https://doi.org/10.3208/sandf1972.15.29.

Itasca, 2015. PFC3D.

Lobo-Guerrero, S., Vallejo, L.E., Vesga, L.F., 2006. Visualization of crushing evolution in granular materials under compression using DEM. Int. J. Geomech. 6, 195–200. https://doi.org/10.1061/(ASCE)1532-3641(2006)6:3(195).

McDowell, G.R., 2002. On the yielding and plastic compression of sand. Soils Found. 42, 139–145.

McDowell, G.R., de Bono, J.P., 2013. On the micro mechanics of one-dimensional normal compression. Géotechnique 63, 895–908. https://doi.org/10.1680/geot.12.P.041.

McDowell, G.R., Nakata, Y., Hyodo, M., 2002. On the plastic hardening of sand. Géotechnique 52, 349–358. https://doi.org/10.1680/geot.2002.52.5.349.

Mitchell, J.K., Soga, K., 2005. Fundamentals of Soil Behavior, 3rd ed. John Wiley and Sons, Hoboken, New Jersey.

Nakata, Y., Kato, Y., Hyodo, M., Hyde, A.F., Murata, H., 2001. One-dimensional compression behaviour of uniformly graded sand related to single particle crushing strength. Soils Found. 41, 39–51.

Pestana, J.M., Whittle, a. J., 1995. Compression model for cohesionless soils. Géotechnique 45, 611–631. doi:10.1680/geot.1995.45.4.611.

Vermeer, P.A., 1978. A double hardening model for sand. Géotechnique 28, 413–433. https://doi.org/10.1680/geot.1978.28.4.413.

Wood, D.M., 1990. Soil Behaviour and Critical State Soil Mechanics. Cambridge University Press.

Yan, W.M., Shi, Y., 2014. Evolution of grain grading and characteristics in repeatedly reconstituted assemblages subject to one-dimensional compression. Géotechnique Lett. 4, 223–229. https://doi.org/10.1680/geolett.14.00039.

Yasufuku, N., Murata, H., Hyodo, M., 1991. Yield characteristics of anisotropically consolidated sand under low and high stresses. Soils Found. 31, 95–109. https://doi.org/10.3208/sandf1972.31.95.